CHAPTER 2

THEORETICAL BACKGROUND: THIN FILM PHOTOVOLTAICS

2.1 Introduction

In this study, attention was focussed on the growth and characterization of semiconductor thin films based on Cu-In-Se, which are applied as absorber films in thin film solar cell devices. Alloys of this semiconductor are variations in which some of the indium (In) is replaced by gallium (Ga) in order to obtain $CuIn_{1-x}Ga_xSe_2$ or where some of the selenium (Se) is replaced by sulfur (S) to obtain $CuIn(Se_{1-x}S_x)_2$. This chapter reviews the material properties of $CuInSe_2$ and its alloys, as well as the state-of-art processing techniques available to produce these chalcopyrite thin films. A brief description of the basic processing steps involved during the fabrication of thin film solar cells and modules will also be given.

2.2 Material Properties of $CuInSe_2$

2.2.1 Crystallographic structure of chalcopyrite compounds

The crystal structure of ternary I-III-VI_2 compounds such as $CuInSe_2$ is well established to be chalcopyrite at room temperature. It belongs to the chalcopyrite family of alloys with space group $I\bar{4}2d$ and transforms to the sphalerite structure at 805ºC. For crystals containing two different atoms in the primitive cell, the structure becomes zinc-blende, with ZnS as the prototype (see Fig. 2.1 (a)).The tetragonal structure of $CuInSe_2$ (see Fig. 2.1(b)), results from the stacking of two cubic zinc-blende structures along the *c*

direction. The primitive cell for this structure is made up of eight tetrahedrons with shared vertices, so that the whole cell is just two stacked cubes. By convention, the short edge is labelled *a* and the long edge is labelled *c*. This gives rise to the condition that, given perfect tetragonal symmetry, $c/a = 2$. It is distinguished from the zinc-blende structure of the binary Grimm-Sommerfield compounds [Grimm and Sommerfield, 1926] by ordering of its face centred cubic (fcc) cation sublattice into distinct sites, one occupied in the ideal structure by copper and the other by indium, and valency considerations require exactly equal numbers of each. The chalcogenide (Se) atoms are located on another fcc lattice referred to as the anion sublattice. The two sublattices interpenetrate such that the four nearest neighbouring sites lie on the anion sublattice, and conversely the four nearest neighbouring sites to each anion site lie on the cation sublattice.

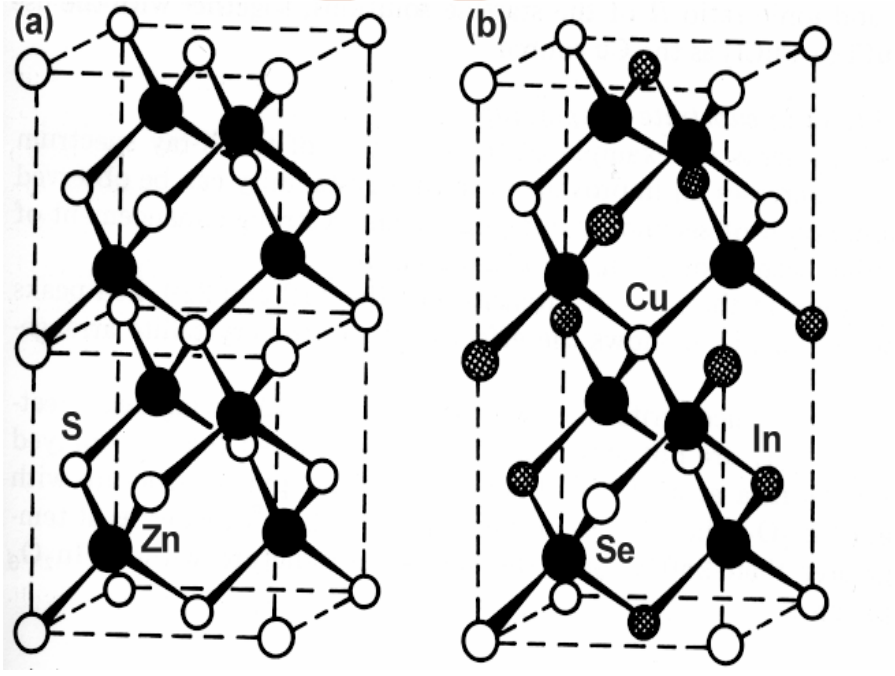

Figure 2.1: Chalcopyrite unit cell for $CuInSe_2$. For the purpose of comparison the closely related zinc-blende ZnS lattice is also depicted.

The tetrahedral coordination of the chalcopyrite lattice gives the structure its sp^3 hybrid covalent bonding with some ionic properties because of the difference in the chemical nature of the atoms [Zunger and Jaffe, 1983]. This bond-length alternation has the electronic effect of reducing the band gap energy of the compound with a chalcopyrite structure, relative to that of the ternary sphalerite structure with identical chemical composition. This band gap reduction effect is known as optical bowing. The lattice constant of $CuInSe_2$ has been widely studied and the early results by Spiess and co-workers [Spiess et al., 1974] are in excellent agreement with the most recent measurements of bond lengths [Chang, 1999]. Typically these values are *a* = 5.784 Å, *c* = 11.616 Å.

2.2.2 Phase diagram of Cu-In-Se

The most common phase of the Cu-In-Se alloy is the α-phase with stoichiometric composition of $CuInSe_2$. The morphology of this compound strongly depends on the processing conditions, and there are several techniques available as outlined in Section 2.3. There are different versions of the phase diagram which describe the possible phases of the Cu-In-Se system [Boehnke and Kuhn, 1987; Koneshova et al., 1982 and Fearheiley, 1986]. However, most of them consider the stoichiometric phase of $CuInSe_2$ as falling along the Cu_2Se-In_2Se_3 tie line on the ternary phase field of this system. One such pseudo-binary phase diagram is shown in Fig. 2.2. According to this phase diagram, various compounds (e.g. $Cu_2In_4Se_7$, $CuIn_3Se_5$, Cu_5InSe_4 and $CuInSe_2$) are likely to occur in this ternary system [Fearheiley, 1986]. The homogeneity region, deduced from x-ray diffraction studies at room temperature, are indicated below the break in the temperature axis. The γ, γ', and γ'' regions represent distinct phases

associated with the compounds $CuInSe_2$, $Cu_2In_4Se_7$ and $CuIn_3Se_5$, respectively. The chalcopyrite single-phase $CuInSe_2$ extends from a stoichiometric composition of 50 mole % In_2Se_3 to In-rich composition of about 55 mole % In_2Se_3. The corresponding Cu/In atomic ratio for this single-phase region lies between 1.0 and 0.82. This tolerance in composition on the In-rich side is one of the factors that make alloys of $CuInSe_2$ attractive candidates for solar cells. For the case where the Cu/In atomic ratios are greater than 1.0, the materials are expected to contain secondary phases of Cu_2Se and for contrary cases (Cu/In atomic ratio less than 0.82) the materials are expected to contain secondary phases of the type $Cu_2In_4Se_7$ and $CuIn_3Se_5$. The Cu_2Se phase is a p-type semiconductor and its presence renders thin films unsuitable for solar cells.

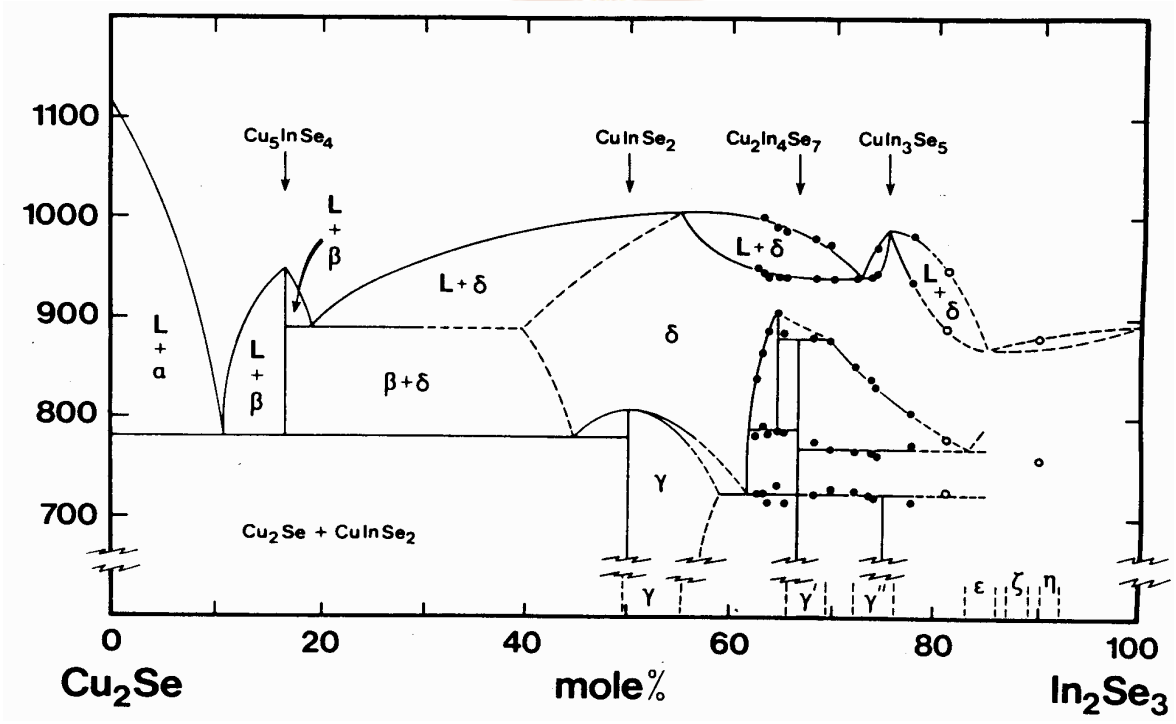

Figure 2.2: Cu_2Se-In_2Se_3 pseudobinary phase diagram [Fearheiley, 1986].

2.2.3 Optical properties

Photovoltaic interest in $CuInSe_2$ and related compounds is largely due to the extremely high absorption coefficient, α, possessed by these materials (see Fig. 2.3). This high value of α ($10^5 cm^{-1}$) implies that 99% of the incoming photons are absorbed within the first micrometer of the material. As a result, only about $1\mu m$ of this material is required to effectively absorb the incoming photons.

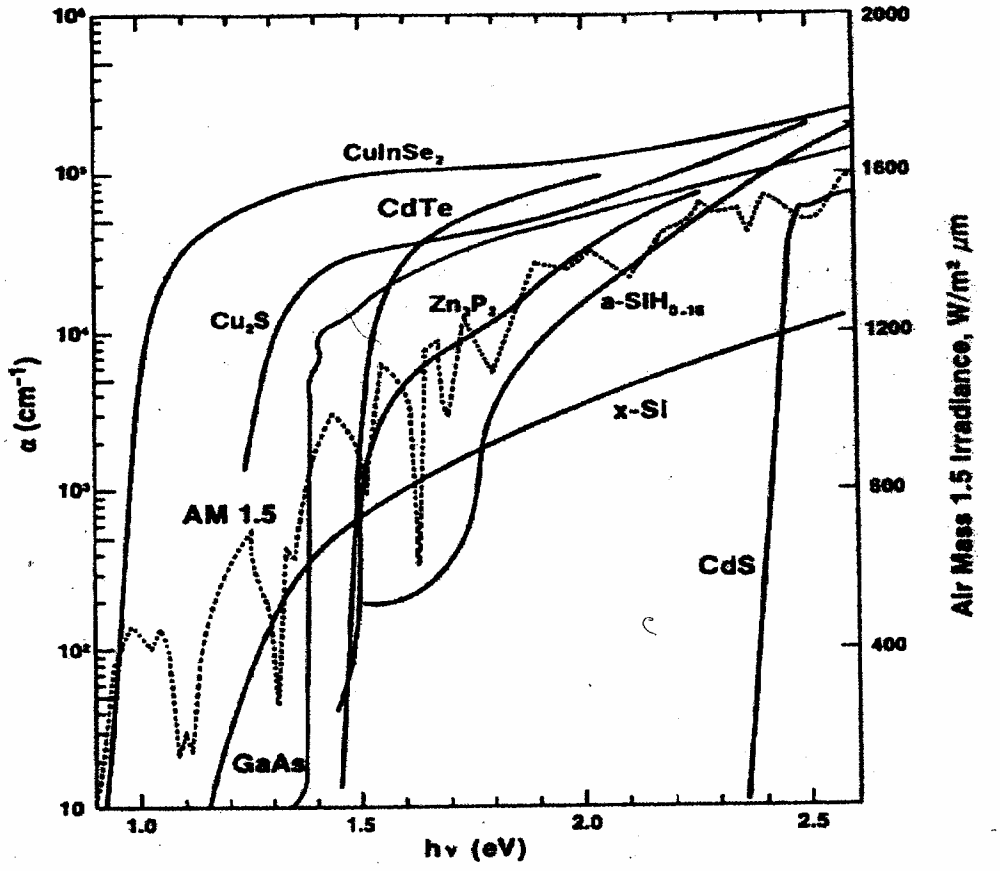

Figure 2.3: Absorption spectrum of $CuInSe_2$ compared with other photovoltaic semiconductors [Jaffe and Zunger, 1984].

Early measurements of the band gap of single-crystalline $CuInSe_2$ exhibited nominal discrepancies [Parkes et al., 1973 and Shay et al., 1973], suggesting a value in the

range of 1.02 to 1.04 eV. Optical characterization of polycrystalline $CuInSe_2$ absorbers films, suitable for devices, almost always indicate a significantly lower effective band gap of approximately 0.9 eV [Kazmerski et al., 1976]. These variations in the optical properties of $CuInSe_2$ materials are a direct consequence of variations in composition between the various samples of single-crystalline crystals and thin films.

Although the direct band gap of $CuInSe_2$ is well suited for fabrication of thin film solar cell devices, a band gap of about $1.2-1.3$ eV is considered optimal for maximizing conversion efficiencies. There have been attempts to modify the band gap of $CuInSe_2$ to better suit the solar spectrum. In one such modification, gallium has been used to replace an indium in the film to form $Cu(In_{1-x}Ga_x)Se_2$. The band gap of the resultant film varied between 1.0 and 1.65 eV for values of x between 0 and 1 and was found to be linearly related to the amount of Ga in the film.

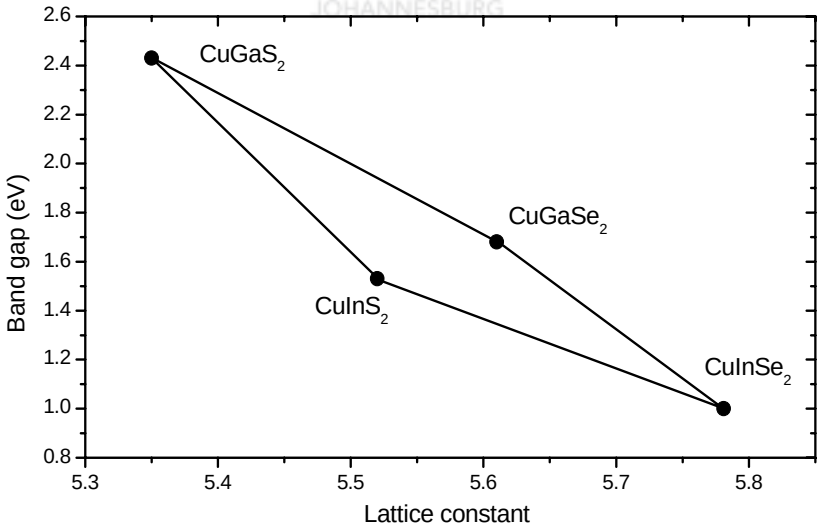

Figure 2.4: Band gap versus lattice constant in angstroms for various chalcopyrite semiconductors.

In another modification, $CuIn(Se_{1-x},S_x)_2$ alloys have been produced by the systematic substitution of selenium (Se) with sulfur (S) atoms. $CuInS_2$ has a band gap of about 1.55 eV and the band gap of $CuIn(Se_{1-x},S_x)_2$ ranges from 1.0 to 1.55 eV, depending on the amount of S in the film. The high flexibility in the optical properties of these chalcopyrite thin films is illustrated in Fig. 2.4. It is important to mention that band gap engineering was also an important aspect of this study in order to improve the device characteristics of solar cell devices.

2.2.4 Defect structure and electrical properties

Intrinsic defects

Pure α-CIS is amphoteric and its conductivity type and carrier density varies with composition. Conceptually the densities of defect structures found in a single-phase material system in equilibrium must be determined uniquely by composition, temperature and pressure. The starting point for atomistic analyses of the defect chemistry of $CuInSe_2$ is the paper by Groenink and Janse [Groenink and Janse, 1978] in which they outlined a generalized approach for ternary compounds based on the elaboration of an earlier model development specifically for spinels by Schmalzried [Schmalzried, 1965]. The number of arbitrary combinations of possible lattice defects (vacancies, antisites, and interstitials) in a ternary system is so vast that useful insight can only be gained by some approximation. Antisite defects created by putting anions on cation sites or vice versa are reasonably neglected because of their extremely high formation energies. The requirement that the crystal as a whole is electrically neutral also leads naturally to Schmalzried's assumption that for any given combination of the thermodynamic variables the concentrations of some pair of defects with opposite signs

will be much higher than the concentrations of all other defects. Groenink and Janse referred to these as the “majority defect pairs”. It is important to note that their treatment assumes that these pairs behave as non-interacting point defects, hence in this context these are “pairs” only in the sense that they occur in roughly equal numbers. It is also significant that this pair dominance implies those conduction processes in these materials should inevitability be characterized by significant electrical compensation, deep level ionised impurity scattering, or both.

The generalized approach by Groenink and Janse was applied specifically to I-III-VI_2 compounds by Rincon and Wasim [Rincon and Wasim, 1986] who derived the proper form for the parameters most useful for quantifying the deviation of the composition of these compounds or alloys from their ideal stoichiometric value:

$$\Delta m = \frac{[I]}{[III]} - 1 \qquad \text{molecular deviation} \qquad (2.1)$$

$$\Delta s = \frac{2[VI]}{[I] + 3[III]} - 1 \qquad \text{valence stoichiometric deviation} \qquad (2.2)$$

Note that in the notation employed in these equations [*I*], for example, denotes the Group I atom fraction. Since [*I*] + [*III*] + [*VI*] = 1, these two deviation variables uniquely specify the solid solution composition. In the same way that a sum rule enables the composition of any ternary mixture to be specified completely using only two of its three fractional compositions, the composition can alternatively be specified by two variables Δm and Δs. The merit of molecularity and valency deviations as an intrinsic relevant

compositional measure in CIS has been empirically demonstrated by careful studies of conductivity in single crystal $CuInSe_2$ [Neumann and Tomlinson, 1990]. Neumann and Tomlinson demonstrated that within the range $|\Delta m| < 0.08$ and $|\Delta s| < 0.06$, p-type conductivity occurs whenever $\Delta s > 0$ (electron deficiency), whereas n-type conductivity occurs for $\Delta s < 0$ (electron surplus).

Electrical Properties

Polycrystalline thin film semiconductors can have electrical properties, which differ significantly from the single crystal behaviour. This is due to the influence of the grain boundaries, which become increasingly important when the grain sizes are in the micron range or below, typical for polycrystalline thin films. Experimental results and theoretical considerations indicated that the important parameters, which determine the electrical behaviour, are the microstructure such as the grain boundary and composition, the grain boundary trap distribution in the forbidden band gap and the doping level. In addition, the electrical properties of the polycrystalline chalcopyrite thin films have been reported to be critically dependent on the method of preparation and annealing treatments after fabrication [Kazmerski and Wagner, 1988]. The important electro-optical parameters of absorbers for photovoltaic applications are the carrier concentration and mobility, which determine the conductivity, absorption and recombination processes. The electrical properties are dominated by the presence of native defects resulting from deviations from stoichiometric composition, as described by equations 2.1 and 2.2. The understanding of electrical transport in polycrystalline chalcopyrite films thus provides the basis for an understanding of the electrical behaviour in general. Hall measurements have confirmed that the change in specific

resistance or conductivity $\sigma = e (n\mu_n + p\mu_p)$ is mainly due to a change of the majority carrier concentration (n or p) and is accompanied by an overall change in Hall mobility. A systematic study of the resistivity and carrier concentration as a function of the composition of the films has been carried out [Noufi et al., 1984]. The composition of the films during the evaporation of the films has been determined by changing the ratio Δm = [Cu]/[In], the molecularity, while maintaining the selenium concentration. Typical results are depicted in Fig. 2.5 (a), which shows that in a narrow range of compositions the carrier concentration drops by several orders of magnitude and the conductivity changes from n- to p-type behaviour. The effect of the selenium/metal (i.e. Se/(Cu+In) ratio) on the carrier concentration for a p-type film in the single-phase region is illustrated in Fig. 2.5 (b) for two fixed Cu/In ratios (Δm = -0.02 and -0.04). $CuInSe_2$ films with Cu in excess of 25 atomic percent are generally p-type. Also selenium-rich films (more than 50 atomic percent) should yield p-type material. In-rich and selenium deficient films, or $\Delta s<0$, are n-type. The conversion of p- to n-type material in general corresponds to a strong decrease in the carrier concentration and conductivity. For solar cell applications the conductivity of the polycrystalline thin film is difficult to control because of the sensitivity to the composition. In order to achieve high efficiency $ZnO/CuInSe_2$ heterojunction solar cell devices, a p-type absorber with an optimum carrier concentration of about 10^{16}-$10^{17}cm^{-3}$ is required.

(a) (b)

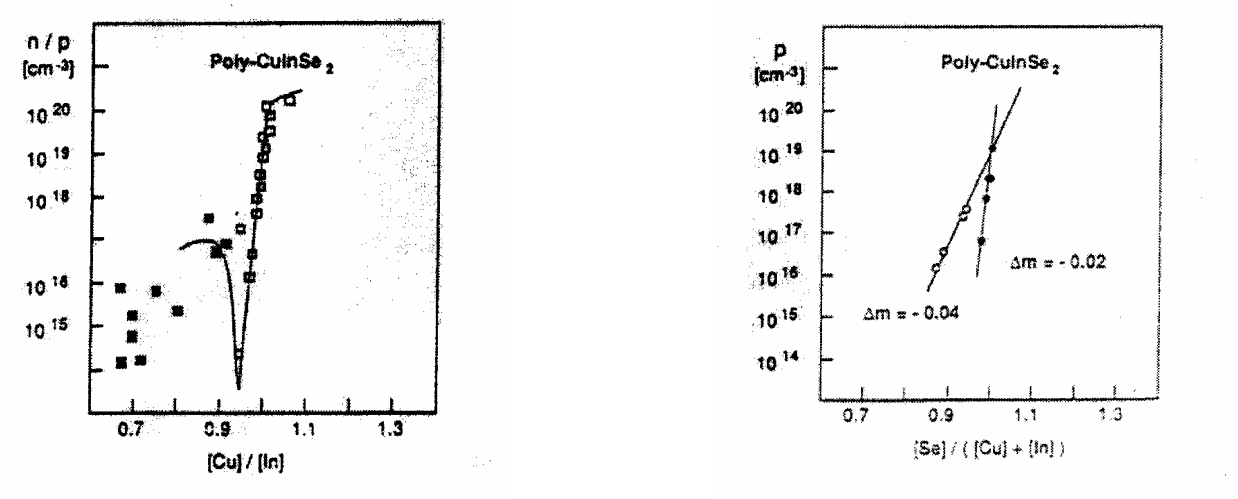

Figure 2.5: (a) Carrier concentration of p- and n-type $CuInSe_2$ single crystals as a function of the composition $\Delta m = [Cu]/[In]$. Solid symbols n-type, open symbols p-type; (b) Majority carrier (hole) concentration of $CuInSe_2$ single crystals as a function of the ratio [Se]/[Cu+In] for two molecularity values $\Delta m = [Cu]/[In]$ [Noufi et al., 1984].

2.3 Processing Techniques for Chalcopyrite Thin Films

$CuInSe_2$ was first synthesized in 1953 [Hahn et al., 1953]. Since then a variety of industrial related growth methods have been developed for the deposition of $CuInSe_2$ based absorbers. The methods can be divided into two major categories:

- Those processes where Se is incorporated with the metals during material delivery, and
- Those where the metals are delivered separately from Se.

Both these processes require thermal activation of Se. Examples of case one are co-evaporation of the three to five elements in vacuum [Tuttle et al., 1995], electrodeposition [Pern et al., 1991], chemical dipping [Garg et al., 1988], chemical vapour deposition [Philibert et al., 1991], spray pyrolysis [Mooney and Lamoreaux, 1986] and sputtering [Devaney and Michelson, 1986; Rockett et al., 1988; Sammann et al., 1980 and Thornson et al., 1988]. Thermal mixing of the stacked binary or elemental layers [Sachan and Meakin, 1993], selenization of CuIn alloy using H_2Se [Schon et al., 1996] or elemental selenium vapour [Lakshmikumar and Rastogi, 1994 and Yamanaka et al., 1993] are examples of case two.

Factors that affect the process selection are the degree of control the process offers, material utilization, capital equipment costs and stability prospects. The most successful methods for depositing device quality films are co-evaporation and the selenization of metals and compound materials in a Se-containing atmosphere. The other techniques have not yet produced high-efficiency devices and/or are not compatible with large-scale production. The most important features and advantages of the co-evaporation and selenization methods are reviewed below.

Multi-source co-evaporation

To date, the simultaneous or co-deposition from elemental sources has been the most successful approach to deposit a variety of chalcopyrite thin films including $CuInSe_2$, $Cu(In,Ga)Se_2$, $CuInS_2$ and $CuIn(Se,S)_2$. In this technique, the composition of the evaporated flux is continuously adjusted from highly copper-rich to highly indium-rich during the growth period. The final overall bulk composition of the film is copper deficient and the surface of the film appears to be terminated by an ordered vacancy

compound (OVC) [Schmid et al., 1993]. The elemental depth profile of these films does not reveal a detectable Cu gradient. As a result, researchers have concluded that the clearly faceted large grained microstructure resulting from the large Cu flux at the early stages of the film growth is maintained during the latter stages and is more conducive to higher conversion efficiencies. $CuInSe_2$ films prepared by this approach thus display the large grain size of a copper-rich material with the desirable electronic properties of the indium-rich compound [Gabor, 1995]. The advantage of this method is the ability to adjust and control the elemental fluxes and substrate temperatures throughout the film deposition process. In principle, S may be incorporated into the absorber using a co-deposition process to obtain films with the general chemical formula of $Cu(In_{1-x}Ga_x)(Se_{1-y}S_y)_2$. Such systems are difficult to synthesize, however, and do not give encouraging results primarily because of excessive shunting and less expected improvement in the open-circuit voltage. Although simultaneous evaporation from four elemental sources has produced the highest total area efficiency of 18.1%, the scale up of co-evaporation has been questioned regarding issues such as material utilization, composition uniformity over large areas, deposition control and throughput [Contreras et al., 1999 and Gillespie et al., 1997]

Selenization process

Another extremely successful processing approach involves the selenization of CuIn alloys in H_2Se. In the most commonly used variation, Cu and In layers of appropriate thickness are first deposited onto molybdenum coated glass substrate. The Cu-In bilayers may be deposited by electro-deposition, evaporation or sputtering. In a second step, this multi-layer precursor structure is annealed in a H_2Se/Ar atmosphere at

temperatures ranging between 350 - 550°C for about 60 to 90 minutes. Variation of this absorber formation technique includes cases where Cu/In/Se or $InSe_x$/Cu thin films structures are used as precursor, and Se vapour and even inert gases are used as annealing atmospheres [Nadeneau et al., 1995 and Alberts et al., 1997]. Even though typical two-step process produces devices with lower efficiencies than that of co-evaporation processes, it has attracted considerable attention because it is thought to be easier to use on a large scale. Siemens Solar Industries (SSI) in the United States developed a process in which sputtered metal precursor layers (Cu/In/Ga) are selenized in H_2Se/Ar. The introduction of H_2S gas in the final stages of the reaction resulted in small area cell efficiencies of around 14% [Gay et al., 1994]. Single-phase device quality $CuInSe_2$ has also been reported by other groups, which included the Institute of Energy Conversion (IEC), the International Solar Electric Technology (ISET) and the National Renewable Energy Laboratory (NREL). The claimed advantages to this approach are:

- Greater process control due to the sequential deposition of the source materials;
- Greater freedom in the choice of the separate deposition techniques during the precursor preparation stage, as well as in the reaction stage enabling processes more adapted to large area, low cost consideration, and
- The potential for higher “quality” of the final material due to thermodynamic equilibrium of the process [Sato et al., 1993; Basol and Kapur, 1990].

2.4 Diffusion Processes and Reaction Kinetics of $CuInSe_2$

The growth of chalcopyrite thin films is controlled by diffusion and reaction processes. Interdiffusion and diffusion in thin films are not basically different from what occurs in bulk specimens. The geometry of thin films and the presence of numerous defects in comparison with bulk materials, induced during processing, make diffusion in thin films a complicated field of study [Phillips, 1990]. Diffusion in thin films can be observed at temperatures well below those at which equilibrium vacancy diffusion is negligible [Hall and Morabito, 1996]. Some of the special characteristics of thin films which may affect diffusion are:

- All volume elements are in close proximity to a free surface, a grain boundary or an interphase boundary;
- Films generally contain high densities of structural defects;
- Large biaxial stresses in the plane of the film are often present;
- Relatively high concentrations of impurities may be present as a result of specific film preparation techniques, and
- Steep chemical and electrostatic gradients may exist.

Structural defects which influence self and impurity diffusion through thin films include grain boundaries, dislocations and vacancies. Grain boundaries are surface or area defects that constitute the interface between grains of different crystallographic orientation. The atoms on the grain boundary are as energetic as the atoms on the film surface and various atomic phenomenon such as diffusion are accelerated. In $CuInSe_2$ thin films, characterized by typical grain sizes around 1μm and a high density of grain boundaries, this effect is expected to play a significant role. The fraction of atoms associated with grain boundaries is roughly $3a_{ad}/l$ where "a_{ad}" is the atomic dimension

and l is the grain size [Ohring, 1992]. Dislocations can be viewed as line defects that bear a definite crystallographic relationship to the lattice. Dislocations can be sites for charge recombination or generations as a result of uncompensated dangling bonds. Diffusion, film stress and thermal induced mechanical relaxation processes are strongly influenced by dislocations. Vacancies are point defects that arise when lattice sites are unoccupied by atoms. Vacancies are formed as the energy required to displace an atom from the lattice to the surface, E_f, is not particularly high. Additionally, the increase in system disorder or entropy due to mixing vacancies among the lattice sites gives rise to a thermodynamic probability that a fraction, f, of the total number of sites will be unoccupied at any temperature, T.

Recent efforts in copper indium diselenide solar cells research have been focused toward understanding the reaction kinetics of copper/indium precursor films. The information is necessary because:

- A complete understanding of the reaction pathways can be used to modify the absorber layer properties for maximum efficiency, and
- The information can be used in the design and the operation of large scale solar panel manufacturing equipment.

Different workers have identified the processes of formation of $CuInSe_2$ when the three constituent elements are heated together in a reaction tube. At first copper and indium elements are independently selenized giving the possible reactions [Sachan and Meakin, 1993]:

(i) $2Cu + Se \rightarrow Cu_2Se$ (133°C)

(ii) $Cu_2Se + Se \rightarrow 2CuSe$ (225°C)

(iii) $3Cu + 2Se \rightarrow Cu_3Se_2$ (500°C)

(iv) $2In + Se \rightarrow In_2Se$ (210°C)

(v) $2In + 3Se \rightarrow In_2Se_3$ (250°C) and

(vi) $In_2Se + Se \rightarrow 2InSe$ (215°C).

The respective compounds then react to form chalcopyrite $CuInSe_2$. In the present study, $CuInSe_2$ and $Cu(In,Ga)Se_2$ thin films were prepared by the selenization of selenium-containing structures (e.g., InSe/Cu and GaSe/Cu/InSe).

2.5 Design and Fabrication of CIS Based Solar Cell Devices

2.5.1 Introduction

A photovoltaic device has to perform two basic functions. The first function is to absorb the incident photons with energy greater than the band gap energy of the material in order to generate electron-hole pairs. The second function is to separate these electron-hole pairs in space in order for a current to flow through an external circuit for utilization. The design and processing of thin film solar cells involve numerous materials and processing parameters, each of which can produce at least 5% variation in the output of the cell [Rothwarf, 1987]. The key issues to the successful fabrication of high efficiency solar cells are easily scalable deposition processes for the active layers, a compatible substrate and suitable contact materials that are controllable or self-regulating [Rothwarf, 1987].

2.5.2 Structure of the heterojunction solar cell

The typical structure for a high-efficiency I-III-VI_2 compound solar cell is shown in Figure 2.6. The commonly used substrate for this device is Mo coated soda-lime glass. It is widely reported that this polycrystalline material adheres better to soda-lime rather than Corning glass. This observation is generally associated with a better match in the thermal coefficients and/or the diffusion of alkali metal from soda-lime glass into the layers (Rockett et al., 1994). The deposition of a thin (1µm) molybdenum layer onto the glass substrate by electron-beam evaporation or sputtering is the first step in the fabrication process. The Mo layer acts as the ohmic back contact to the cell and also improves the adhesion between the glass substrates and the active layers. Selection of Mo as the contact material for $CuInSe_2$ is due to its relative stability under $CuInSe_2$ film growth conditions (i.e. it does not chemically interfere with the growing film at the processing temperatures). However, the quality of the $CuInSe_2$ film (i.e. morphology, grain size and orientation) is directly affected by the quality of the underlying Mo layers. If the Mo layer is deposited under sub-optimized conditions, it exhibits either tensile or compression stresses which contribute to the commonly observed peeling of $CuInSe_2$ films at the Mo/$CuInSe_2$ interfaces. The key component of the solar cell configuration, depicted in Figure 2.6, is the polycrystalline absorber film. The performance characteristics of polycrystalline $CuInSe_2$ materials are strongly influence by grain size, grain orientation, loss mechanisms originating from grain boundaries, and crystal defects. Besides losses due to insufficient diffusion lengths, photo-generated carriers can recombine at grain boundaries and/or the hetero-interfaces (i.e. Mo/$CuInSe_2$, $CuInSe_2$/CdS, CdS/ZnO) due to lattice mismatches which cause interface states. The electrical and optical properties of compound films are highly dependent on their

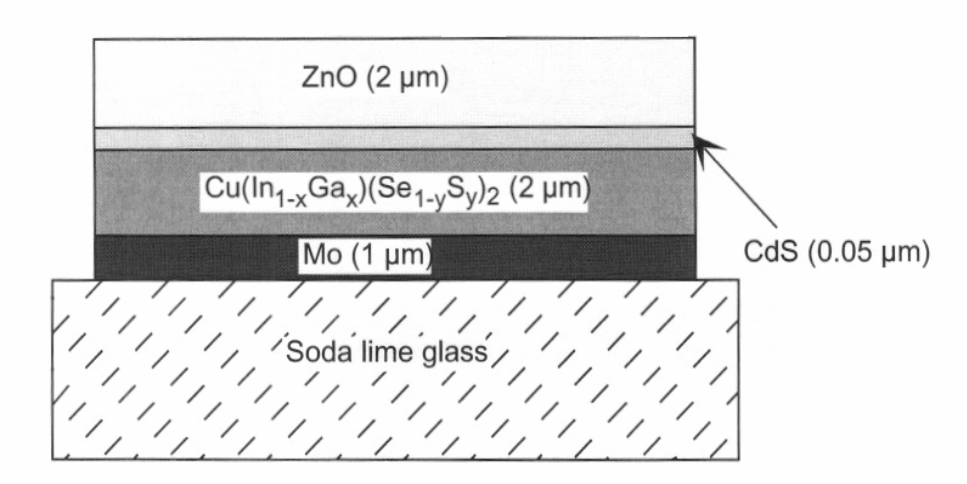

Figure 2.6: Typical Structure of a $CuInSe_2$.

stoichiometric composition, defect chemistry and structure which in turn are strongly related to the film growth parameters.

The heterojunction is formed between the absorber film and a n-type ZnO window layer. In order to improve device performance, a 50 nm thick CdS buffer layer is deposited between the absorber and window layers. The CdS buffer layer is lattice and electronically matched to the $CuInSe_2$ absorber film and its presence controls the density of interface states and prevents the inter-diffusion of species (i.e. Cu, In or Se) from the absorber into the ZnO window layer, and vice versa. It is also believed that these buffer layers passivate the grain boundaries of the polycrystalline $CuInSe_2$ absorber films, resulting in high open circuit voltages. The CdS buffer are prepared by a chemically bath deposition (CBD) technique. The primary advantage of this method is that complete surface coverage of the rough polycrystalline absorber films is obtained at very low CdS thickness, typically 5-10 nm. Standard evaporation techniques require much thicker films (> 1µm) to obtain complete surface coverage, which results in a significant absorption in the CdS layer and subsequently a reduction in the blue

response of completed solar cell devices. ZnO is the ideal window material due to its wide band gap (3.2 eV), high temperature stability and the fact that it can be doped in any desired order. The ZnO window layers are deposited by means of DC or RF sputtering at temperatures below 200^{o}C. The use of $n^{+}p$ heterojunctions shifts the electrical junction (i.e. the position within the space charge region where the density of electrons equals the density of holes) away from the metallurgical interface into the absorber. Therefore, photo-generated electrons crossing the metallurgical interface from the absorber into the ZnO window layers are majority carriers at this interface and thus are less affected by recombination. The solar cell structure is completed by the evaporation of 1-2 μm thick Al grid contacts onto the ZnO window layer. In order to reduce resistive losses, a 50 nm thick Ni layer can be included between the ZnO window layer and the Al grid contacts. Although not shown in Figure 2.6, a MgF_2 anti-reflection coating is normally incorporated into the structure to limit reflective losses.

2.5.3 Module fabrication processes

The technologies for absorber, buffer and window layer deposition used for module production are the same as those discussed for the production of small laboratory cells. However, the challenges of research on modules are to transform the laboratory-scale technologies to a much larger area. The relative high substrate temperatures that are necessary for high-quality materials impose problems in handling very large area glass sheets. Future process optimization therefore implies reduction of the substrate temperature.

One inherent advantage of thin-film technologies for photovoltaics is the possibility of using monolithic integration for series connection of individual cells within a module.

The interconnect scheme, shown in Figure 2.7, has to ensure that the ZnO of one cell is connected to the Mo back contact of the next cell. Three different patterning steps are necessary to obtain these connections. The first interrupts the Mo back contact by a series of periodical scribes and thus defines the width of the cell, which is about 5 – 10 mm. The second patterning is performed after the absorber and CdS buffer deposition, and the final one after the ZnO window layer deposition. The final interconnect width is of the order of 300 µm. Thus about 3 – 5 % of the cell area is sacrificed for interconnection. Module efficiency is directly impacted by active area losses, which is related to the scribe width and spacing. The positional accuracy and minimum line width that can be obtained for individual scribes determine the scribe spacing. Accurate positioning registration, reproducibility and fine line width are required to minimize active area losses. The module is then completed by laying an encapsulant, such as ethyl vinyl acetate (EVA, a thermosetting thermoplastic used religiously within the photovoltaic field), over the cells, covering it with another piece of glass and cutting the EVA. Finally, current leads are attached to the contacts for external connections.

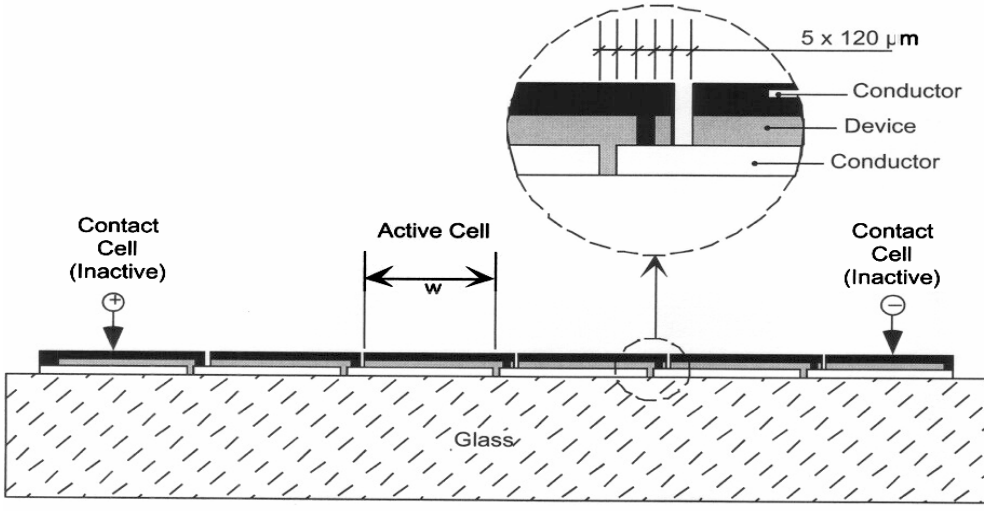

Figure 2.7: Schematic cross-section view of a polycrystalline thin film photovoltaic module.

References

Alberts V., Zweigart S., Schon J. H. and Schock H. W., *Semicond. Sci. Technol*. **12,** p. 217, (1997).

Basol B. M. and Kapur V. K., Proc. 21st IEEE PV Specialists Conference (Kissiminee, USA), p. 418, (1990).

Boehnke V. C. and Kuhn G., *Journal of Material Science* **22**, p. 1635, (1987).

Chang C. -H., Dissertation, University of Florida, (1999).

Contreras M. A., Egaas B., Ramanathan K., Hiltner J., Swartzlander A., Hasoon F. and Noufi R., (1999) " *Pro. Photovoltaic Res, Appl.* **7**, pp. 311-316, (1999).

Devaney W. E. and Michelson R. A., *Solar Cells* **16**, p. 131, (1986).

Fearheily M. L., *Solar* Cells **16**, p. 91, (1986).

Gabor R. A., The conversion of $(In,Ga)Se_3$ Thin Films to $Cu(In,Ga)Se_2$ for application to Photovoltaic solar cells, Ph.D. Thesis, University of Colorado, (1995).

Garg J. C., Sharma R. P. and Sharma K. C., *Thin Solid Films* **164**, p. 269, (1988).

Gay R., Dietrich m., Fredric C., Jensen C., Knapp K., Terrant D. and Willet D., Proceedings of the 12th European Photovoltaic Solar Energy Conference (Amsterdam), p. 935, (1994).

Gillespie T. J., Lanning B. R. and Marshall C. H., Proc. IEEE 26th Photovoltaic Specialist Conference (Anaheim, USA), p. 403, (1997).

Grimm H. G. and Sommerfield A., *Z. Phys*. **36**, p. 439, (1926).

Groenink A. and Janse P. H., *Zeitschrift fur Physicalishe Chemie Neue Folge* **110**, p. 17 (1978).

Hahn H., Frank G., Klinger W., Meyer A. D. and Storger G. Z., *Anorrg. Allchem. Chem* **271**, p. 153, (1953).

Hall P. M. and Morabito J. M., *Thin Solid Films* **33**, p. 107, (1996).

Jaffe J. E. and Zunger A., *Phys. Review* **29** (4), pp. 1882-1905, (1984).

Kazmerski L. L. and Wagner S., *Current Topics in Photovoltaic*, Academic Press, New York **3**, p. 79, (1988).

Kazmerski L. L., White F. R. and Morgan G. K., *Applied Physics Letters* **29**, p. 268, (1976).

Koneshova T. I., Babitsyna A. A. and Kalinnikov V. T., Izvestiya Akademii Nauk SSSR, *Neorganicheskie Materialy* **18**, p. 1483, (1982).

Lakshmikumar S. T. and Rastogi A. C., Solar Energy Mater. *Solar Cells* **32**, p. 7, (1994).

Mooney J. B., and Lamoreaux R. H., *Solar Cells* **16**, p. 211, (1986).

Nadeneau V., Braunger D., Harikos D., Kaisar M., Kobel C. H., Oberacker A., Ruckh M., Ruhle U., Schaffer R., Schmid D., Walter T., Zweigatt S. and Schock H. W., *Prog. Photovolt*. **3**, p. 363, (1995).

Neumann H. and Tomlinson R. D., *Solar Cells* **28**, p. 301 (1990).

Noufi R., Axton R., Herrington C. and Deb S. K., *Appl. Phys. Lett*. **45**(6), p. 668, (1984).

Ohring M., The Material Science Thin Films, (Academic Press, Inc., New York), (1992).

Parkes J., Tomlinson R. D. and Hamphire M. J., *Solid State Electronics* **16**, p. 773 (1973).

Pern F. J., Noufi R., Mason A. and Franz A., *Thin Solid Films* **202**, p. 299, (1991).

Philibert J., Pattee G. H., Cosslett V. E. and Engstrom A., Proc. 34rd Intl. Symp. X-ray Optics and X-ray Microanalysis, Stanford University. Academics Press, New York, p. 379, (1991).

Phillips J. E., Proc. 21st IEEE Photovoltaic Specialists Conference (Las Vegas, USA), p. 1614, (1990).

Rincon C. and Wasim S. M., Proc. 17th International Conference, (Materials Research Society, Pittsburgh), p. 443, (1986).

Rockett A., Abou-Elfotouh., Albin D., Bode M., Klenk R., Lommasson T. C., Russell T. W. F., Tomlinson R. D., Tuttle J., Stolt L., Walter T. and Peterson T. M., *Thin Solid Films*, **237** (1-2), p. 1-11, (1994).

Rockett A., Lommasson T. C., Yang L. C., Talieh H., Campos P. and Thornton J. A., Proc. 20th IEEE Photovoltaic Specialist Conference(Las Vegas, USA), p. 1505, (1988).

Rothwarf A., S*olar Cells* **21**, p. 1, (1987).

Sachan V. and Meakin J. D., *Solar Cell*s **30**, p. 147, (1993).

Sammann A. N. Y., Abdul-Karim N., Abdul-Hussein N., Tomlinson R. D., Hill A. E. and Armour D. G., *Jpn J. Appl. Phys*. **19**(3), p. 15, (1980).

Sato H., Hama T., Niemi E., Ichikawa Y. and Sakai H., Proc. 23rd IEEE Photovoltaic Specialists Conference (Louisville, USA), p. 521, (1993).

Schmalzried H., *Progress in Solid State Chemistry* **2**, p. 265, (1965).

Schmid D., Ruch M., Grunward F. and Scholk H. W., *J. Appl. Phys*. **73**(6), p. 2902, (1993).

Schön J. H., Alberts V. and Bucher E., *J. Appl. Phys*. **81** (6), p. 2799, (1996).

Shay J. L., Tell B., Kasper M. K. and Schiavone L. M., *Physical review* **7**, p. 4485 (1973).

Spiess H. W., Haeberlen U., Brandt G., Rauber A. and Schneider J., *Physica Status Solidi* (b) **62**, p. 183, (1974).

Thornson J. A., Lommasson T. C., Taileh H., and Tseng B. H., *Solar Cells* **24**, p. 1, (1988).

Tuttle J. R., Contreras M. A., Gillespies T J., Ramanathan K. R., Tennant A. L., Keanne J., Gabor A. M., and Noufi R., *Prog. Photovolt*. **3**, p. 235, (1995).

Yamanaka S., McCandles B., and Birkmire R. W., Proc. 23rd IEEE photovoltaic Specialists Conference, (Louisville, USA), p. 607, (1993).

Zunger A. and Jaffe J. E., *Physical Review Letters* **51**, p. 662, (1983).